Density functional simulation of the $BaZrO_3$ (011) surface structure

Eugene Heifets,* Justin Ho, and Boris Merinov†
California Institute of Technology, MS 139-74, Pasadena, California 91125, USA
(Received 30 September 2006; revised manuscript received 6 December 2006; published 25 April 2007)

The atomic structure and charge redistribution of different terminations of $BaZrO_3$ (011) surfaces have been studied using density functional simulations. We found that the O-terminated (011) flat surface had the smallest cleavage energy among (011) surfaces, but this value was still twice as large as for the formation of a pair of complimentary (001) surfaces. The density functional calculations allowed us to estimate the excess surface Gibb's free energy and to compare stability of different (011) surfaces as a function of chemical environment. In addition, we compared stability of $BaZrO_3$ (011) surfaces with respect to $BaZrO_3$ (001) surfaces. Within boundaries, where $BaZrO_3$ does not decompose, only the Ba- and O-terminated (011) surfaces appeared to be stable. However, if (001) surfaces are also taken into consideration, the BaO-terminated (001) surface is the only stable surface among all considered (001) and (011) surfaces.

DOI: 10.1103/PhysRevB.75.155431 PACS number(s): 68.35.Bs, 68.35.Md, 68.47.Gh, 73.43.Cd

I. INTRODUCTION

Doped barium zirconate ($BaZrO_3$) is presently considered a very promising proton conducting material, which can be applied in a variety of electrochemical devices, including fuel cells, sensors, electrolysis cells, and hydrogen pumps.[1] $BaZrO_3$ is also used as a substrate for growing high-temperature perovskite superconductors.[2] In all mentioned applications $BaZrO_3$ shares surface contacts with other materials. Detailed information on $BaZrO_3$ surface structures would therefore be very helpful for understanding the structure and behavior of its interfaces with other materials.

To our knowledge, no experimental investigations of $BaZrO_3$ surfaces have been reported yet. Recently, the first computational study of the $BaZrO_3$ (001) surface structure[3] has been performed using density functionals defined in the local density approximation,[4] in the Perdew-Burke-Ernzerhof (PBE) version[5] of the generalized gradient approximation, and within the full potential linearized augmented plane wave method. We performed a similar study[6] with a basis set from localized Gaussian type orbitals while employing a PBE functional. Our study also included a thermodynamic analysis of the relative stability of (001) surfaces with different terminations. Among similar materials the most-studied surfaces are those of $SrTiO_3$. Both crystals, $BaZrO_3$ and $SrTiO_3$, have the same cubic perovskite structure at ambient and elevated temperatures. Formal ionic charges are identical in these crystals. We expect that surface properties of both crystals are similar as well. The $SrTiO_3$ (100) surface relaxation and rumpling have been studied experimentally by means of several powerful techniques: Low energy electron diffraction (LEED),[7] reflective high energy electron diffraction,[8,9] and metastable impact electron spectroscopy.[10] Theoretically, the $SrTiO_3$ (001) surface has been studied by atomistic methods[11–16] and by various first-principle methods.[17–27]

There are two types of (011) crystal planes in perovskites like $BaZrO_3$. One crystal plane contains two oxygen ions in each unit cell, and the other contains single Ba^{2+}, Zr^{4+}, and O^{2-} ions per unit cell. Both of these planes are charged with density of $\pm 4e$ per unit cell (e is the absolute value of the electron charge). If (011) surfaces were prepared by cleaving a $BaZrO_3$ crystal between these planes, the resulting surfaces would be charged. Such surfaces are commonly defined as polar. They are unstable because excess charge density causes spurious electric fields. Stabilization of polar surfaces is possible with a reduction of the charge density at the surfaces. In the case of crystals built from two equidistant nonequivalent charged crystal planes, like in $BaZrO_3$, the charge density must be reduced by half with respect to its bulk value.[28]

Investigations of (011) perovskite surfaces are less common than (001) surfaces. At present only the data for $SrTiO_3$ (011) crystal surfaces are available. The $SrTiO_3$ (110) polar perovskite surface has been studied experimentally using LEED,[29] which showed a number of surface reconstructions at high temperatures. Atomic force microscopy measurements also support the existence of surface modifications resulting from applied extensive thermal treatment.[30,31] However, there are no experimental data on the relaxations of the $SrTiO_3$ (110) surfaces at low temperatures. A few semiempirical quantum mechanical calculations[32,33] have been published for this type of perovskite surfaces. Recently, the atomic relaxations for the polar (110) surfaces of $SrTiO_3$ and $BaTiO_3$ have been studied by atomistic simulations employing the shell model.[34] The local-density approximation method with plane waves was used in the first *ab initio* study of these surfaces.[35] Another *ab initio* study of these $SrTiO_3$ surfaces applied the Hartree-Fock method and localized basis sets built from Gaussian-type atomic orbitals.[36] All theoretical investigations mentioned above examined $SrTiO_3$ (011) surfaces obtained by simply cleaving the crystals between (011) planes or by cleaving and incorporating additional electrostatic stabilization through removal of some surface ions.

Calculations of the total energy allow comparison between different surface configurations with constant chemical composition. However, the composition of perovskite surfaces is subject to variations. Therefore, stabilities of these surfaces can be compared only by means of corresponding thermodynamical potentials. An appropriate model must include exchange of atoms between the surfaces and external reservoirs. This picture corresponds to a standard

large canonical ensemble and is characterized by the Gibbs free energy. The most stable surface has the smallest excess (with respect to the bulk crystal) Gibbs free energy due to the surface creation. This concept was applied in studies of perovskite surfaces by Padilla and Vanderbilt.[17,18] Simple metal oxides (TiO_2 and SrO or BaO) were taken as external reservoirs. The chemical potentials were limited by precipitation of the oxides at the perovskite surface. A similar approach was applied again in Refs. 32 and 35, where the area of $SrTiO_3$ free surface existence was restricted by precipitation on the surface of Sr and Ti metals or by oxygen loss into the surrounding environment. The oxygen in the environment is characterized using its chemical potential. Chemical potentials are not values that can be measured easily. Therefore, it is preferable to express the Gibbs free energies through values accessible in experiments. References 37–40 and 27 provide such an approach which allows the surface excess Gibbs free energy to be expressed through measurable partial pressure and temperature of oxygen gas, combining calculated and experimental data.

Here we report results of our simulations of $BaZrO_3$ (011) surfaces and analyze their structures and surface stabilities at various oxygen partial pressures and temperatures. Possible mechanisms for polar surface stabilization in $BaZrO_3$ are considered in Sec. II A. We also introduce a potential mechanism for stabilization of (011) perovskite surfaces through formation of cation antisite defects. Section II B is devoted to the description of computational techniques applied in our study. The formula for calculations of the energy needed for cleaving a crystal is given in Sec. II C. In Sec. II D we describe a thermodynamical approach employed to analyze stabilities of different perovskite surfaces. Section III contains the description and analysis of all produced results. Section III A describes atomic structures and charge distributions obtained for $BaZrO_3$ (011) surfaces with various terminations. Then in Sec. III B we compare cleavage energies needed for the formation of various pairs of (011) and (001) $BaZrO_3$ surface terminations. Finally, in Sec. III C we use computed slab and bulk unit cell energies to determine stable surfaces of $BaZrO_3$. An analysis of the stability of surfaces with different terminations is performed by comparing excess Gibbs free energies corresponding to the creation of the surfaces.

II. THEORY

A. Polarity compensation and its implications

In the [011] orientation of $BaZrO_3$, the atomic layers are stacked -O_2-BaZrO-O_2-BaZrO-. Crystal planes with the [011] orientation are not electrically neutral, regardless of whether atomic charges are calculated using Mulliken population analysis or estimated with formal ionic charges. Therefore, the creation of (011) surfaces introduces polarity, which tends to create instability due to surplus surface charges or dipole moments and resultant spurious electric fields. Assuming that the ionic charges of O, Ba, and Zr are equal to formal charges ($Q_O=-2e$, $Q_{Zr}=+4e$, and $Q_{Ba}=+2e$), the O_2 layers would bear a charge of $\sigma_{O2}=-4e$ per unit cell area, while the BaZrO planes would bear a charge with density $\sigma_{BaZrO}=+4e$ per unit cell area. Such surfaces can become

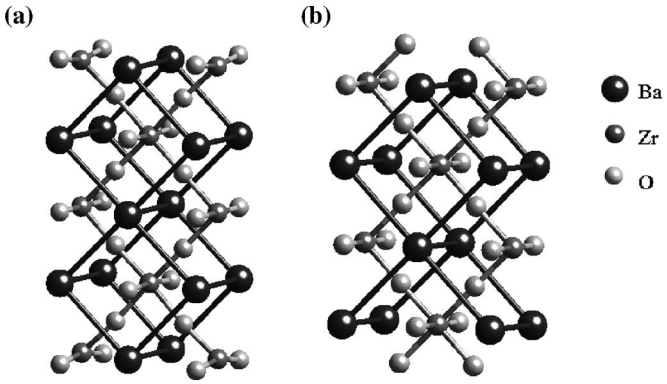

FIG. 1. Unit cells of slabs employed for simulation of (011)-oriented $BaZrO_3$ surfaces, the *stoichiometric* terminations: (a) BaZrO-terminated slab or (b) O_2-terminated slab.

stable if the surface charge density is adequately reduced to prevent the appearance of infinite potentials and spurious electric fields. Due to this condition (the condition of polarity compensation[28]), the formal surface charge density of the possible $BaZrO_3$ (011) surfaces have to be equal to one-half of the bulk value; that is, the charge compensation must be presented in such a way that $\sigma_{surface}=\pm 2e$.

To address the necessity for polarity compensation, three types of terminations can be considered (Figs. 1–3). One type consists of the *stoichiometric* terminations with surface planes having the same composition as in the bulk planes: The (011) BaZrO-terminated and (011) O_2-terminated slabs (Fig. 1). Since changes in surface stoichiometry are not introduced to compensate the surface charge, the compensation is achieved instead through electron redistribution within several near-surface layers. In nonconducting materials such electron redistribution is usually accompanied by anomalous filling of the surface electron states.

In the second type of terminations for the [011] direction the stoichiometry of the surface planes differs from that of the corresponding plane in the bulk through the removal of one or more atoms. These manipulations result in surfaces with Ba, ZrO, and O terminations (Fig. 2). In these *nonstoichiometric* cases, the charged defects should, in principle, be sufficient to remove the excess surface charge and provide the polarity compensation.

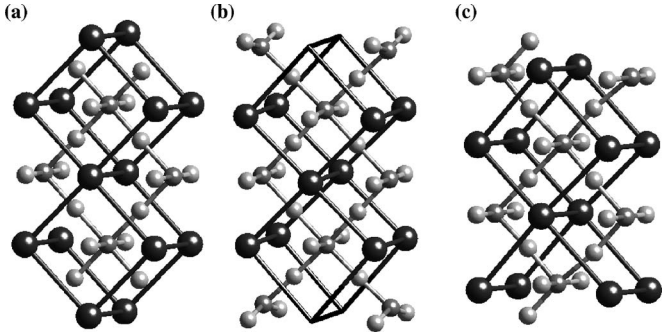

FIG. 2. Unit cells of slabs employed for simulation of (011)-oriented $BaZrO_3$ surfaces, the *nonstoichiometric* terminations: (a) Ba-terminated slab, (b) ZrO-terminated slab, and (c) O-terminated slab.

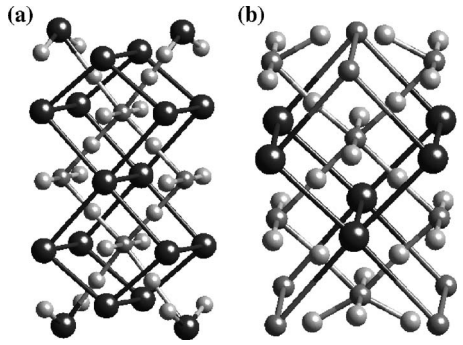

FIG. 3. Unit cells of slabs employed for simulation of (011)-oriented $BaZrO_3$ surfaces, the *substitution* terminations: (a) Ba_2O-terminated slab and (b) O_2/Zr_2O-terminated slab.

The third type can be described as the exchange of one cation with another (Fig. 3). We refer to this type of termination as *substitution* terminations. In one of the (011) surfaces Ba atoms replace Zr atoms in the top layer of the BaZrO-terminated surface to form a Ba_2O-terminated surface. The complimentary surface consists of an O_2-terminated surface in which a Zr ion substitutes a Ba ion in the subsurface layer. We refer to such a surface termination as "O_2/Zr_2O." In terms of formal charges, this last structure has an outer surface layer charge density of $-4e$, and a charge density at the subsurface layer of $+6e$. When added together the formal charges of these two layers give a value that is half of the bulk layer charge. This value is precisely what is required to stabilize the surface.

B. Method of the total energy computations

We used the SeqQuest computational code[41] to perform the ab initio electronic structure calculations. This code allows efficient computations of electronic structures for systems with different dimensionalities (0D–3D) and with local Gaussian-type basis sets. Local basis sets allow application of truly two-dimensional (2D) slab computations without introducing artificial periodicity in the third direction. In our simulations the PBE (Ref. 5) functional was employed. The core electrons were replaced with pseudopotentials. The norm-conserving pseudopotentials[42] were created using the ionic electronic structure computed with the PBE functional as well. The oxygen pseudopotential belongs to the Troullier-Martins type[43] and replaces core electrons. The basis set[42] for oxygen valence electrons was "double zeta" quality and included polarization basis functions of d symmetry. Hamann type[44] pseudopotentials were used for Ba and Zr. Non-linear core correction[45] was included in the Zr pseudopotential. For both atoms p electrons of the last core shell were not included into the pseudopotentials and were treated explicitly in the same way as the valence electrons. The basis set[42] for these atoms included also functions of s and d symmetries. The basis sets for Ba and Zr were also of "double zeta" quality. Charges of ions were computed using the Mulliken population analysis.

In the beginning of our simulations we optimized a lattice constant for a bulk cubic $BaZrO_3$ crystal. These computations used an $8\times8\times8$ mesh in a Brillouin zone for integrations in reciprocal space. We obtained a value of the lattice constant equal to 4.244 Å, while the experimental value[47] is 4.182 Å. The calculated band gap of 3.10 eV is significantly underestimated with respect to the experimental value of 5.0 eV (Ref. 48) or 5.33 eV,[49] which is quite usual for DFT calculations. The optimized value of the lattice constant was used in our subsequent simulations of the surfaces. We also calculated energy per unit cell for barium and zirconium oxides in the most stable low-temperature phases (BaO in the rocksalt phase and ZrO_2 in the monoclinic phase). These values were necessary for estimating a region of existence of free $BaZrO_3$ surfaces. Computational conditions were the same as in the $BaZrO_3$ bulk calculations. Unit cells for both BaO and ZrO_2 were optimized[6] as well.

The surfaces were modeled using symmetrical nine-layered 2D slabs (Figs. 1–3). The slabs were oriented perpendicular to the [011] crystal direction. Terminations were the same on both sides of the slabs. All studied terminations of $BaZrO_3$ (011) surfaces are described in Sec. II A. Integrations over the first Brillouin zone were performed using an 8×8 mesh. Positions of the atoms were optimized keeping mirror symmetry of the slabs with respect to the slab central plane. The computational conditions were identical to those used in our previous calculations[6] for $BaZrO_3$ (001) surfaces.

C. Cleavage energies

When a crystal is cleaved, two complementary surfaces are created. Bringing them back together restores the crystal structure. Complementary pairs of surfaces with O_2 and BaZrO terminations and with Ba and ZrO terminations are possible for the (011) surface orientation. The O-terminated surface is complementary to itself. Here we consider Ba_2O and O_2/Zr_2O terminated surfaces as complementary as well, even though it requires returning antisite Zr and Ba cations to their own sites in addition to joining the surfaces in order to restore the perfect crystal structure.

In present simulations we use symmetric slabs terminated with the same surfaces on both sides. Since the thickness of the slabs is nine layers, two slabs with complementary terminations brought together will have a total thickness equal to nine crystal unit cells. To create these two slabs two cleaves are needed. Cleavage energy is the energy required to cleave a crystal. Therefore, computations of the cleavage energies per surface unit cell were calculated using

$$E_{\text{cleave}}(j,j') = -\frac{1}{2}[E^{j}_{\text{slab}} + E^{j'}_{\text{slab}} - 9E^{\text{bulk}}_{\text{BaZrO}_3}], \tag{1}$$

where $E^{\text{bulk}}_{\text{BaZrO}_3}$ is the total energy per unit cell of $BaZrO_3$ and E^{j}_{slab} and $E^{j'}_{\text{slab}}$ are the total energies per surface unit cell for complementary slabs. The cleavage energy density per unit area is equal to

$$\varepsilon_{\text{cleave}}(j,j') = \frac{E_{\text{cleave}}(j,j')}{A}, \tag{2}$$

where A is the surface unit cell area.

D. Surface stability analysis

The cleavage energy is a measure of the energy required to split a crystal into two parts with complementary terminations. It does not account for the possibility of ion exchange between a crystal and its surrounding environment. Therefore, they cannot be used for studying stability of different surfaces at various chemical conditions. This analysis has to be made with surface Gibbs free energy (SGFE) which is a measure of the excess energy of a semi-infinite crystal in contact with matter reservoirs.[17,18,27,32,35,37–40] SGFEs are functions of chemical potentials of different atomic species. The most stable surface has a structure with the smallest SGFE among all possible surface structures.

Introducing the chemical potentials μ_{Ba}, μ_{Zr}, and μ_{O} for the Ba, Zr, and O atomic species, respectively, SGFE per unit cell area Ω^i corresponding to the $\boldsymbol{i}$ termination is defined as

$$\Omega^i = \frac{1}{2}[G^i_{\mathrm{slab}} - N^i_{\mathrm{Ba}}\mu_{\mathrm{Ba}} - N^i_{\mathrm{Zr}}\mu_{\mathrm{Zr}} - N^i_{\mathrm{O}}\mu_{\mathrm{O}}], \tag{3}$$

where N^i_{Ba}, N^i_{Zr}, and N^i_{O} denote numbers of Ba, Zr, and O atoms in the slab. SGFE per unit area is represented by

$$\omega^i = \frac{\Omega^i}{A}. \tag{4}$$

The chemical potential $\mu_{\mathrm{BaZrO_3}}$ of barium zirconate is equal to the sum of the chemical potentials of each atom type in $BaZrO_3$ crystal:

$$\mu_{\mathrm{BaZrO_3}} = \mu_{\mathrm{Ba}} + \mu_{\mathrm{Zr}} + 3\mu_{\mathrm{O}}. \tag{5}$$

Due to requirement for the surface of each slab to be in equilibrium with the bulk barium zirconate, the chemical potential is equal to the bulk crystal Gibbs free energy that gives the expression

$$\mu_{\mathrm{BaZrO_3}} = g^{\mathrm{bulk}}_{\mathrm{BaZrO_3}}. \tag{6}$$

We can simplify the equation for the SGFE and eliminate the chemical potentials μ_{Zr} and $\mu_{\mathrm{BaZrO_3}}$ by substituting this expression for the $BaZrO_3$ bulk chemical potential:

$$\Omega^i = \frac{1}{2}[G^i_{\mathrm{slab}} - N^i_{\mathrm{Zr}} g^{\mathrm{bulk}}_{\mathrm{BaZrO_3}}] - \Gamma^i_{\mathrm{Zr,Ba}}\mu_{\mathrm{Ba}} - \Gamma^i_{\mathrm{Zr,O}}\mu_{\mathrm{O}}, \tag{7}$$

where $\Gamma^i_{\mathrm{Zr},a}$ are the excesses in the $\boldsymbol{i}$ terminated surface of components a with respect to the number of Zr ions in slabs:[27]

$$\Gamma^i_{\mathrm{Zr},a} = \frac{1}{2}\left(N^i_a - N^i_{\mathrm{Zr}}\frac{N^{\mathrm{bulk}}_a}{N^{\mathrm{bulk}}_{\mathrm{Zr}}}\right). \tag{8}$$

To keep barium and zirconium atoms from leaving the bulk of a $BaZrO_3$ crystal and precipitating on the surface, their chemical potentials have to be less than the Gibbs free energy of corresponding metals:

$$\mu_{\mathrm{Ba}} \leqslant g^{\mathrm{bulk}}_{\mathrm{Ba}}, \tag{9}$$

$$\mu_{\mathrm{Zr}} \leqslant g^{\mathrm{bulk}}_{\mathrm{Zr}}. \tag{10}$$

Similarly, precipitation of oxides does not occur if

$$\mu_{\mathrm{Ba}} + \mu_{\mathrm{O}} \leqslant g^{\mathrm{bulk}}_{\mathrm{BaO}}, \tag{11}$$

$$\mu_{\mathrm{Zr}} + 2\mu_{\mathrm{O}} \leqslant g^{\mathrm{bulk}}_{\mathrm{ZrO_2}}. \tag{12}$$

The Gibbs free energies per unit cell for crystals are defined as

$$g^{\mathrm{bulk}}_j = E_j + E^{\mathrm{vibr}}_j - Ts_j + pv_j, \tag{13}$$

where E_j is a static component of the crystal energy, E^{vibr}_j is a vibrational component of the crystal energy, v_j is volume, and s_j is entropy. All these values are given per molecule in crystal j. We can reasonably assume that applied pressure is not larger than ~100 atm in practical cases. The largest volume per molecule in a crystal among materials considered here is in $BaZrO_3$ and equal to ~73 Å^3. Then the largest pv_j term in Eq. (13) can be estimated as ~5 meV. This value is much smaller than the amount of uncertainty in our DFT computations and, therefore, can be safely neglected. As is commonly practiced, we will neglect the vibration contributions to g^{bulk}_j, including contributions from zero-point oscillations to the vibrational part of the total energy. Estimates made in Ref. 38 demonstrate that the changes in the vibrational part of the total energy due to temperature are nearly compensated by changes in the entropy. Therefore, we approximate the Gibbs free energies with the total energies obtained from DFT calculations:

$$g^{\mathrm{bulk}}_j \approx E^{\mathrm{bulk}}_j. \tag{14}$$

Introducing deviations for the Ba and Zr chemical potentials,

$$\Delta\mu_{\mathrm{Ba}} = \mu_{\mathrm{Ba}} - g^{\mathrm{bulk}}_{\mathrm{Ba}} \approx \mu_{\mathrm{Ba}} - E^{\mathrm{bulk}}_{\mathrm{Ba}} \tag{15}$$

and

$$\Delta\mu_{\mathrm{Zr}} = \mu_{\mathrm{Zr}} - g^{\mathrm{bulk}}_{\mathrm{Zr}} \approx \mu_{\mathrm{Zr}} - E^{\mathrm{bulk}}_{\mathrm{Zr}}, \tag{16}$$

from their values in the bulk metals, equilibrium condition Eq. (5) can be rewritten as

$$\Delta\mu_{\mathrm{Ba}} + \Delta\mu_{\mathrm{Zr}} + 3\Delta\mu_{\mathrm{O}} = \Delta g_f(\mathrm{BaZrO_3}), \tag{17}$$

where

$$\Delta g_f(\mathrm{BaZrO_3}) = g^{\mathrm{bulk}}_{\mathrm{BaZrO_3}} - g^{\mathrm{bulk}}_{\mathrm{Ba}} - g^{\mathrm{bulk}}_{\mathrm{Zr}} - \frac{3}{2}E_{\mathrm{O_2}}$$

$$\approx E^{\mathrm{bulk}}_{\mathrm{BaZrO_3}} - E^{\mathrm{bulk}}_{\mathrm{Ba}} - E^{\mathrm{bulk}}_{\mathrm{Zr}} - \frac{3}{2}E_{\mathrm{O_2}}. \tag{18}$$

Here $\Delta g_f(\mathrm{BaZrO_3})$ has the meaning of the Gibbs free energy of formation for $BaZrO_3$ from Ba, Zr, and O_2 in their standard states. Boundary conditions (9)–(12) are transformed into

$$\Delta\mu_{\mathrm{Ba}} \leqslant 0, \tag{19}$$

$$\Delta\mu_{\mathrm{Ba}} + 3\Delta\mu_{\mathrm{O}} \geqslant \Delta g_f(\mathrm{BaZrO_3}), \tag{20}$$

$$\Delta\mu_{\mathrm{Ba}} + \Delta\mu_{\mathrm{O}} \leqslant \Delta g_f(\mathrm{BaO}), \tag{21}$$

$$\Delta\mu_{\mathrm{Ba}} + \Delta\mu_{\mathrm{O}} \geqslant \Delta g_f(\mathrm{BaZrO_3}) - \Delta g_f(\mathrm{ZrO_2}), \tag{22}$$

where

$$\Delta g_f(\mathrm{BaO}) = g^{\mathrm{bulk}}_{\mathrm{BaO}} - g^{\mathrm{bulk}}_{\mathrm{Ba}} - \frac{1}{2}E_{\mathrm{O}_2} \approx E^{\mathrm{bulk}}_{\mathrm{BaO}} - E^{\mathrm{bulk}}_{\mathrm{Ba}} - \frac{1}{2}E_{\mathrm{O}_2} \tag{23}$$

and

$$\Delta g_f(\mathrm{ZrO_2}) = g^{\mathrm{bulk}}_{\mathrm{ZrO_2}} - g^{\mathrm{bulk}}_{\mathrm{Zr}} - E_{\mathrm{O}_2} \approx E^{\mathrm{bulk}}_{\mathrm{ZrO_2}} - E^{\mathrm{bulk}}_{\mathrm{Zr}} - E_{\mathrm{O}_2} \tag{24}$$

are the Gibbs free energies of formation for barium and zirconium oxides.

Oxygen in $BaZrO_3$ is in equilibrium with oxygen gas in the atmosphere over the crystal surface, leading to equality of oxygen chemical potentials in a crystal and in the atmosphere:

$$\mu_{\mathrm{O}} = \frac{1}{2}\mu^{\mathrm{gas}}_{\mathrm{O}_2}. \tag{25}$$

Chemical potentials are hard to access in experimental and industrial conditions. It is much more convenient to work with gas temperatures and pressures. In addition, the oxygen gas chemical potential is highly dependent on gas temperature and oxygen partial pressure. Therefore, we use this dependence to express the Gibbs free energies for $BaZrO_3$ surfaces through temperature and oxygen gas partial pressure. Oxygen gas at the considered conditions can be treated in very good approximation as an ideal gas. Therefore, dependence of its chemical potential from pressure can be expressed as[27,38]

$$\mu^{\mathrm{gas}}_{\mathrm{O}_2}(T,p) = \mu^{\mathrm{gas}}_{\mathrm{O}_2}(T,p^0) + kT\ln\left(\frac{p}{p^0}\right), \tag{26}$$

where k is the Boltzmann constant. Here p^0 is some reference pressure which we can take as the standard pressure. We can evaluate the temperature dependence of $\mu_{\mathrm{O}_2}{}^{\mathrm{gas}}(T,p^0)$ using experimental data, as has been done previously in Refs. 27 and 38. For this we define the reference state as an isolated oxygen molecule E_{O_2}. Changes in the chemical potential for the oxygen atom can be written as

$$\begin{aligned}\Delta\mu_{\mathrm{O}}(T,p) &= \mu_{\mathrm{O}}(T,p) - \frac{1}{2}E_{\mathrm{O}_2} \\ &= \frac{1}{2}\left\{\Delta G^{\mathrm{gas}}_{\mathrm{O}_2}(T,p^0) + kT\ln\left(\frac{p}{p^0}\right)\right\} + \delta\mu^0_{\mathrm{O}}.\end{aligned} \tag{27}$$

Here $\Delta G_{\mathrm{O}_2}{}^{\mathrm{gas}}(T,p^0)$ is a change in the oxygen gas Gibbs free energy at the pressure p^0 and temperature T with respect to its Gibbs free energy at $T^0=298.15$ K

$$\begin{aligned}\Delta G^{\mathrm{gas}}_{\mathrm{O}_2}(T,p^0) &= G^{\mathrm{gas}}_{\mathrm{O}_2}(T,p^0) - G^{\mathrm{gas}}_{\mathrm{O}_2}(T^0,p^0) \\ &= H^{\mathrm{gas}}_{\mathrm{O}_2}(T,p^0) - H^{\mathrm{gas}}_{\mathrm{O}_2}(T^0,p^0) - TS^{\mathrm{gas}}_{\mathrm{O}_2}(T,p^0) \\ &\quad + T^0S^{\mathrm{gas}}_{\mathrm{O}_2}(T^0,p^0).\end{aligned} \tag{28}$$

TABLE I. Variations in Gibbs free energy for oxygen gas at standard pressure ($p^0=1$ atm) with respect to its value at 0 K. Data are taken from thermodynamical tables (Ref. 46).

T (K)	$\Delta G_{\mathrm{O}_2}{}^{\mathrm{gas}}(T,p^0)$ (eV)	T (K)	$\Delta G_{\mathrm{O}_2}{}^{\mathrm{gas}}(T,p^0)$ (eV)
100	−0.07	1000	−1.10
200	−0.17	1100	−1.23
250	−0.22	1200	−1.36
298.15	−0.27	1300	−1.49
300	−0.27	1400	−1.62
400	−0.38	1500	−1.75
500	−0.50	1600	−1.88
600	−0.61	1700	−2.02
700	−0.73	1800	−2.16
800	−0.85	1900	−2.29
900	−0.97	2000	−2.43

The experimental data for oxygen gas enthalpy $H_{\mathrm{O}_2}{}^{\mathrm{gas}}$ and entropy $S_{\mathrm{O}_2}{}^{\mathrm{gas}}$ as functions of temperature at standard pressure can be taken from the standard thermodynamical tables.[46] We present calculated values for $\Delta G_{\mathrm{O}_2}{}^{\mathrm{gas}}(T,p^0)$ in Table I.

$\delta\mu^0_{\mathrm{O}}$ in expression (28) is a correction which should bring experimental data and results of quantum-mechanical computations in line. This correction was estimated from computations of metal oxides and metals in a way similar to the approach applied in Ref. 27. Enthalpy of an M_xO_y oxide can be written as

$$h^0_{M_x\mathrm{O}_y} = xh^0_M + \frac{y}{2}h^0_{\mathrm{O}_2} + \Delta H^0_{f,M_x\mathrm{O}_y}. \tag{29}$$

Here enthalpies of the oxide, $h^0_{M_x\mathrm{O}_y}$, and of the metal, h^0_M, can be approximated by the total energies for these materials calculated at 0 K on the same grounds that we used for approximation (14). Heats of formation for BaO and ZrO_2 (in the most stable monoclinic phase) at standard conditions are equal to 548.1 kJ/mol and 1097.46 kJ/mol, respectively.[46] Equation (29) allows estimation of the standard oxygen gas enthalpy. Since we define the total energy of an oxygen molecule as zero for chemical potential and enthalpy calculations, a correction for the enthalpy has to be defined as

$$\delta h^0_{\mathrm{O}_2} = h^0_{\mathrm{O}_2} - E_{\mathrm{O}_2}. \tag{30}$$

Taking the experimental standard entropy for oxygen as $S^0_{\mathrm{O}_2}=205.147$ J mol^{-1} K^{-1},[46] the desired correction to the oxygen chemical potential can be calculated using the equation

$$\delta\mu^0_{\mathrm{O}} = \frac{1}{2}(\delta h^0_{\mathrm{O}_2} - T^0S^0_{\mathrm{O}_2}) = \frac{1}{2}(h^0_{\mathrm{O}_2} - E_{\mathrm{O}_2} - T^0S^0_{\mathrm{O}_2}). \tag{31}$$

Finally, we can rewrite Eq. (7) as

$$\Omega^i = \phi^i - \Gamma^i_{\mathrm{Zr,Ba}}\Delta\mu_{\mathrm{Ba}} - \Gamma^i_{\mathrm{Zr,O}}\Delta\mu_{\mathrm{O}}, \tag{32}$$

where

$$\phi^i = \frac{1}{2}[G^i_{\text{slab}} - N^i_{\text{Zr}} g^{\text{bulk}}_{\text{BaZrO}_3}] - \Gamma^i_{\text{Zr,Ba}} g^{\text{bulk}}_{\text{Ba}} - \frac{1}{2}\Gamma^i_{\text{Zr,O}} E_{\text{O}_2}$$

$$\approx \frac{1}{2}[E^i_{\text{slab}} - N^i_{\text{Zr}} E^{\text{bulk}}_{\text{BaZrO}_3}] - \Gamma^i_{\text{Zr,Ba}} E^{\text{bulk}}_{\text{Ba}} - \frac{1}{2}\Gamma^i_{\text{Zr,O}} E_{\text{O}_2} \quad (33)$$

resembles the expression for Gibbs free energy of surface formation. We calculated SGFE for all surfaces described in Sec. II A employing Eqs. (32) and (33). The region where $BaZrO_3$ surfaces are stable with respect to precipitation of Ba or Zr metals or their oxides is determined by inequalities (19)–(22). The surface with the greatest stability for different values of $\Delta\mu_{\text{Ba}}$ and $\Delta\mu_{\text{O}}$ has the smallest SGFE.

If SGFE becomes negative, surface formation will lead to an energy gain. The surface will form spontaneously and the crystal will be destroyed. Therefore, the condition for sustaining a crystal structure is for SGFE to be positive for all potential surface terminations. The boundary for the region of existence for a bulk crystal can be found by solution of the equation

$$\Omega^i(\Delta\mu_{\text{Ba}}, \Delta\mu_{\text{O}}) = 0, \quad (34)$$

where i corresponds to the surface with the lowest SGFE.

III. RESULTS AND DISCUSSION

A. Electronic and atomic structure of (011)-oriented surfaces

1. Stoichiometric terminations

(a) *BaZrO termination*. In the stoichiometric (011) BaZrO termination (Fig. 1) anomalous filling of surface states is required to remove the excessive surface charge. In the study of the analogous (011)-SrTiO terminated surface of $SrTiO_3$ in Ref. 35 the Fermi energy was found to be located above the conduction band bottom, indicating that some states in the conduction band were occupied. The two additional electrons that are needed according to the rule for polarity compensation occupy states at the bottom of the conduction band near the surface. The surface becomes metallized. The band structure cannot be computed within the SeqQuest code employed here.[41] However, a negligible band gap of 0.004 eV was found for the BaZrO-terminated surface in this study, suggesting that the BaZrO terminated surface is indeed metallized (see Table II). The polarity compensation can be verified by means of Mulliken charge analysis, as shown in Table III. The layer charge of the first and third BaZrO planes and the second O_2 plane are strongly modified, as compared to the computed charge for the bulk crystal planes, suggesting filling of the additional surface states. Layer charges comparable to those of the bulk are established somewhat by the fourth layer. The polarity compensation condition is fulfilled, since the sum of the charges on the first four layers comes out to $+1.111e$, which is roughly half of the bulk layer charge, Q^{bulk}. One can also see from Table III that the difference between the surface layer charge and the bulk layer charge is mainly localized on the barium. This is somewhat surprising given that Ba has more ionic character than Zr, whose Mulliken charge should be more susceptible to change due to its propensity for varying degrees of covalent interactions with neighboring oxygen atoms.

TABLE II. Band gaps for different surface terminations. The values were calculated as differences between energies of the last occupied and the first vacant electron levels. Computations were made at the nodes of the 8×8 mesh in Brillouin zone. Data for (001) surfaces are taken from Ref. 6.

Termination	Band gap (eV)
BaZrO (011)	0.004
O_2 (011)	0.79
Ba (011)	1.54
ZrO (011)	3.01
O (011)	2.92
Ba_2O (011)	0.49
O_2/Zr_2O (011)	0.75
BaO (001)	3.04
ZrO_2 (001)	2.40
Bulk	3.10
Bulk (expt)	5.0,[a] 5.33[b]

[a]Reference 48.
[b]Reference 49.

It is evident from the summary of relaxation in Table IV that the displacements of atoms become relatively small by the third layer. Large relaxations are concentrated in the first two outermost layers. A large rumpling between oxygen and barium in the outermost layer (0.38 Å) is drastically reduced by the third layer (0.17 Å). The interplanar distance between the outermost BaZrO layer and the O_2 subsurface layer contracts by 6%, while the distance between the O_2 subsurface layer and the third BaZrO layer increased by +8%. This phenomenon is typical of the damped oscillation that makes each pair of unlike layers closer.[35]

(b) O_2 *termination*. In O_2-terminated surface Mulliken charges on the surface O ions are about half of their charge in the bulk (see Table III). Two surface oxygen atoms connected to two different Zr atoms, which are neighbors in the (011) orientation, move to a distance of 1.42 Å from one another, forming peroxo ion O_2^{2-}. As usual, calculated quantum-mechanical charges of the surface oxygen atoms are much smaller than their formal charges. Mulliken charges of the surface atoms are equal to $-0.584e$, which is approximately one-half of the value of the oxygen atom charge in the bulk of $BaZrO_3$. Therefore, requirements for polarity compensation are nearly fulfilled already in the first surface layer. Despite the removal of two electrons per unit cell from the valence band, metallization of this surface does not occur. It is prevented because the movement of surface oxygen atoms toward one another causes opening of the band gap of 0.79 eV at the Fermi level. All of these results are very similar to results for $SrTiO_3$.[35]

Surface relaxation and rumpling are much smaller than those observed for $SrTiO_3$ in Ref. 35. Interplanar distances converge very fast with depth into the slab. The distance between the first and the second layers decreases by 13%, and the distance between the second and the third layers

TABLE III. Mulliken charges of Ba, Zr, and O for stoichiometric (011) terminations. I, II, III, IV, and V give the number of the layer counted from the surface. The values in parentheses show deviations from respective values in the crystal bulk.

Layer	Atomic charges (e)			Layer charge per unit cell (e)
	Ba	Zr	O	
BaZrO-*terminated:*				
BaZrO (I)	0.933 (−0.752)	1.711 (−0.196)	−1.172 (0.025)	1.472 (−0.923)
O_2 (II)			−1.176 (0.021)	−2.352 (0.043)
BaZrO (III)	1.618 (−0.067)	1.752 (−0.155)	−1.196 (0.001)	2.175 (−0.220)
O_2 (IV)			−1.203 (−0.006)	−2.406 (−0.011)
BaZrO (V)	1.655 (−0.030)	1.770 (−0.137)	−1.201 (−0.004)	2.224 (−0.171)
O_2-*terminated:*				
O_2 (I)			−0.584 (0.613)	−1.168 (1.227)
BaZrO (II)	1.559 (−0.126)	1.940 (0.033)	−1.184 (0.013)	2.315 (−0.080)
O_2 (III)			−1.189 (0.008)	−2.378 (0.017)
BaZrO (IV)	1.676 (−0.009)	1.944 (0.037)	−1.194 (0.003)	2.426 (0.031)
O_2 (V)			−1.195 (0.002)	−2.390 (0.005)

increases by 2%. Changes in interplanar distances between subsequent layers relative to the bulk are insignificant. The largest rumpling is found in the subsurface layer, where Ba and O ions move outwards by 0.04 and 0.03 Å, respectively, and Zr ion moves inwards by 0.07 Å.

TABLE IV. Interplanar distances and rumpling on stoichiometric (011) terminations. Positions of crystal planes are computed by averaging the coordinates of the corresponding atoms. The interplanar distances are given in angstroms and their variations with respect to the bulk value are provided in parentheses (in percents of interplanar distances in the bulk). Rumpling is determined as the distance between the atom and respective crystal plane.

Layer	Interplanar distances (Å)	Rumpling (Å)		
		Ba	Zr	O
BaZrO-*terminated:*				
BaZrO (I)		−0.16	−0.06	0.22
⇕	1.42 (−6%)			
O_2 (II)				0
⇕	1.62 (+8%)			
BaZrO (III)		−0.09	0.01	0.08
⇕	1.46 (−3%)			
O_2 (IV)				0
⇕	1.53 (+2%)			
O_2-*terminated:*				
O_2 (I)				0
⇕	1.31 (−13%)			
BaZrO (II)		−0.04	0.07	−0.03
⇕	1.54 (+2%)			
O_2 (III)				0
⇕	1.49 (−0.6%)			
BaZrO (IV)		0.002	−0.016	0.014
⇕	1.485 (−1%)			

2. Nonstoichiometric (011) terminations

(a) Ba and ZrO terminations. At first glance, polarity in the (011)-Ba and (011)-ZrO terminations is already compensated by the creation of these defects. Therefore, one would expect that the atomic surface charges undergo little modification from their corresponding atomic charges in the bulk. However, we find that the sum of the Mulliken charges for the surfaces with Ba and ZrO terminations differ significantly from one-half of the crystal plane charge, as required by charge polarity compensation. The reduced coordination numbers of the surface atoms in the Ba- and ZrO-terminated surfaces and the requirement for charge polarity compensation lead to significant changes in the atomic charges (see Table V). The changes spread even as far as the third layer from the surface. In the Ba-terminated surface a partial electron charge comes to the surface Ba ion, causing the Ba ion to lose almost a third of its charge as a result. The charges of two following layers are reduced by approximately the same value ($\sim 0.18e-0.19e$). The difference is less substantial as in the (011)-ZrO terminated surface. The surface Zr atom has the Mulliken charge of $+2.179e$, which is $0.272e$ larger than the Mulliken charge of the corresponding Zr ion in the bulk (Table V). Both removal of the Ba ion and the increase of the surface Zr ion charge are responsible for the most significant changes in the surface layer charge. Although the differences between surface and bulk charges in $BaZrO_3$ are greater than those observed in $SrTiO_3$,[35] the Mulliken charge analysis for both cases indicates that the polarity compensation is fulfilled within the first three outermost layers. The sums of the first three layer charge densities are $+1.21e$ and $+1.19e$ for the ZrO termination and Ba termination, respectively. This is roughly a half of the bulk planar charge value.

The band gap in the ZrO-terminated surface (3.01 eV) is just slightly reduced with respect to the bulk band gap (3.10 eV). In contrast, the band gap in the Ba-terminated $BaZrO_3$ (011) surface decreases to 1.54 eV, reflecting a significantly lower coordination of the surface Ba ions.

Since the atoms in the (011)-ZrO and (011)-Ba terminated (011) surfaces are undercoordinated, they undergo large re-

TABLE V. Mulliken charges of Ba, Zr, and O for nonstoichiometric (011) terminations. I, II, III, IV, and V give the number of the layer counted from the surface. Values in parentheses show deviations from respective values in the crystal bulk.

Layer	Atomic charges (e)			Layer charge per unit cell (e)
	Ba	Zr	O	
Ba-*terminated:*				
Ba (I)	1.184 (−0.501)			1.184 (−1.211)
O_2 (II)			−1.104 (0.093)	−2.207 (0.188)
BaZrO (III)	1.574 (−0.111)	1.851 (−0.056)	−1.209 (−0.012)	2.215 (−0.180)
O_2 (IV)			−1.202 (−0.005)	−2.404 (−0.009)
BaZrO (V)	1.671 (−0.014)	1.949 (0.042)	−1.197 (0.000)	2.423 (0.028)
ZrO-*terminated:*				
ZrO (I)		2.179 (−0.272)	−1.157 (0.040)	1.022 (−1.363)
O_2 (II)			−1.230 (−0.033)	−2.460 (−0.065)
BaZrO (III)	1.703 (−0.018)	2.135 (−0.228)	−1.194 (0.003)	2.644 (0.249)
O_2 (IV)			−1.192 (0.005)	−2.384 (0.011)
BaZrO (V)	1.671 (−0.014)	1.886 (−0.021)	−1.201 (−0.004)	2.356 (−0.039)
O-*terminated:*				
O (I)			−1.144 (0.053)	−1.144 (1.241)
BaZrO (II)	1.504 (−0.181)	2.014 (0.107)	−1.189 (0.008)	2.328 (−0.067)
O_2 (III)			−1.232 (−0.035)	−2.396 (−0.001)
			−1.164 (0.033)	
BaZrO (IV)	1.661 (−0.024)	1.945 (0.038)	−1.197 (0.000)	2.409 (0.014)
O_2 (V)			−1.230 (−0.033)	−2.396 (−0.001)
			−1.165 (0.032)	

laxations, as evidenced by very large inward relaxation of the surface Ba on the Ba termination, and strong rumpling of the Zr and O atoms on the ZrO termination (0.46 Å), both indicated in Table VI. Contrary to the regular pattern, the top surface layer in the ZrO-terminated surface moves outward suggesting that the attraction of this layer to the following layers is decreased. Such unusual relaxation is probably influenced more strongly by the charge reduction in the surface layer than by the requirement for polarity compensation. Despite the undercoordination, the relaxations are quickly damped, as compared to those of the (011) stoichiometric terminations. For instance, the interplanar relaxation between the third and the fourth layer for the Ba and ZrO terminations is nearly negligible, and rumpling effects fade in the third and fourth layers.

(b) O termination. Since the (011)-O termination is intrinsically compensated by the stoichiometry, the surface atomic charges should differ little from the bulk ones. Accordingly, the summary of the Mulliken charges in Table V shows only slight changes in the O atom charge in the surface from its bulk value. Likewise, there are only small fluctuations in the charges of the Zr and Ba atoms from their bulk counterparts in layers close to the surface. Polarity compensation is achieved after the first two layers, as the sum of the charge densities of the surface and subsurface layers is $+1.184e$, which is very close to a half of the bulk layer charge density.

The band gap value (2.92 eV) in the O-terminated surface is smaller than its corresponding bulk band gap value by only ~0.2 eV. There is no reason to expect any significant modification of the $BaZrO_3$ band structure by the surface.

Due to symmetry, the z coordinates of the O atoms in each of the O_2-terminated layers are identical in the slabs corresponding to the other surface types. Therefore, there is no rumpling in O_2 layers in these surfaces. In the O-terminated surface the two oxygen atoms are less constrained and, therefore, rumpling in the O_2 layers below the surface is more attainable (Table VI). The broken symmetry induces instability of ZrO_6 octahedra through rotation, as it is observed in antiferroelectric phases. The octahedral rotation propagates deep into the crystal. Similar propagation of the octahedral rotation was observed in $SrTiO_3$.[34–36] The surface O relaxes inward quite significantly (29%; see Table VI). However, owing to the polarity compensation within the first two layers, the difference in the interplanar spacings between subsequent layers is significantly damped. The change in the interplanar spacing between the second and third layers is only 4%. However, the distortion of the octahedra, as exemplified in the rumpling of the two oxygen atoms in the O_2 layers, continues propagating through the thickness of the slab.

3. Substitution terminations

(a) Ba_2O *termination*. Formation of the (011)-Ba_2O terminated surface requires an environment with a relatively large Ba surplus. The calculated band gap value for the Ba_2O-terminated slab is 0.485 eV. This indicates a significant change in the electronic structure of the surface compared to that of a bulk crystal. We expect appearance of surface bands due to replacement of Zr atoms by Ba atoms.

TABLE VI. Interplanar distances and rumpling on nonstoichiometric (011) terminations. Positions of crystal planes are computed by averaging the coordinates of the corresponding atoms. The interplanar distances are given in angstroms and their variations with respect to the bulk value are provided in parentheses (in percents of interplanar distances in the bulk). Rumpling is determined as the distance between the atom and respective crystal plane.

Layer	Interplanar distances (Å)	Rumpling (Å)		
		Ba	Zr	O
Ba-*terminated:*				
Ba (I)		0		
⇕	1.01 (−33%)			
O_2 (II)				0
⇕	1.56 (+4%)			
BaZrO (III)		0.01	0.00	−0.01
⇕	1.51 (+1%)			
O_2 (IV)				0
⇕	1.51 (+1%)			
ZrO-*terminated:*				
ZrO (I)			−0.23	0.23
⇕	1.57 (+5%)			
O_2 (II)				0
⇕	1.51 (+1%)			
BaZrO (III)		−0.02	0.09	−0.08
⇕	1.42 (−5%)			
O_2 (IV)				0
⇕	1.51 (+1%)			
O-*terminated:*				
O (I)				0
⇕	1.06 (−29%)			
BaZrO (II)		0.01	−0.05	0.04
⇕	1.56 (+4%)			
O_2 (III)				±0.12
⇕	1.49 (−1%)			
BaZrO (IV)		−0.02	0.02	0.00
⇕	1.49 (−1%)			

There is no need for anomalous filling of the surface states of the Ba_2O-terminated surface, because the charge compensation is already provided by the replacement of ions. However, the charge modifications are expected to extend more deeply, especially when the effective charges are considered, given the significant reduction of the surface band gap with respect to the bulk value. In Table VII, the Mulliken charges for the Ba_2O-terminated slab are listed. A significant reduction of the charges on the surface Ba atoms compared to their counterparts in the bulk is observed. Charges of +1.15*e* and +1.04*e* appear on the surface Ba atoms, where a larger charge reduction occurs at the Ba atoms located in the Zr sites. The charge distributions on the atoms contribute to a surface charge density of +1.26*e*. A significant charge density reduction extends over three layers from the surface. Polarity compensation is satisfied through the same first three layers with a charge density sum of +1.183*e*, which is roughly a half of the charge of a bulk layer.

The substitution of ions in the surface layer produces pronounced rumpling effects in the first layer of the Ba_2O-terminated surface. These two Ba atoms are separated by a vertical distance of 1.08 Å. The Ba atom located in the original surface Ba site and the oxygen atom move inward to the slab, but the Ba atom that replaced the Zr atom moves outward. At the same time, a change in the interplanar spacing between the first and second layers is relatively small (7%; see Table VIII). The next interplanar distance increases by 5%. Rumpling of the atoms is greatly reduced progressively deeper within the slab, and changes in the interplanar spacing as compared to the bulk interplanar distance also become negligible.

(b) O_2/Zr_2O *termination*. In contrast to the Ba_2O-terminated surface, the O_2/Zr_2O-terminated surface occurs under Zr-rich and Ba-poor conditions. The band gap in the O_2/Zr_2O-terminated surface is reduced significantly to 0.753 eV. We assume that the reduction of the band gap occurs due to the presence of the surface bands, caused by the replacement of atoms in this surface.

Two top surface layers should provide necessary polarity compensation, if our consideration is limited only to the formal ion charges. Indeed, changes in the atomic charges extend deeply within the O_2/Zr_2O-terminated slab. Modification of the charges at least in the first four surface layers is needed to achieve polarity compensation (see Table VII). Charges of the oxygen atoms decrease in both surface (by 0.23*e*) and subsurface (by 0.04*e*) layers. However, charges of Zr atoms in the subsurface layer increase by 0.15*e* and 0.29*e*, where the smaller change occurs on the Zr atoms in the surface Ba site.

Due to symmetry, the outermost O_2 layer does not undergo any rumpling, and rumpling in the subsurface Zr_2O layer is only 0.27 Å between two Zr atoms (Table VIII). On the other hand, large changes in the interplanar spacing are observed, and remain quite significant through the entire slab. The interplanar spacing between the first two layers is reduced enormously, by 42%, and remains significant between the fourth and fifth layers (12%, see Table VIII). The rumpling in the fourth layer is actually greater than the rumpling observed in the second layer. The difference in the vertical displacements of the Ba and O atoms in the fourth layer is 0.35 Å. Without simulations of slabs with a thickness greater than nine, it is difficult to say whether the rumpling in O_2/Zr_2O-terminated surface and changes in the interplanar distances are damped as they extend farther into the bulk, and how far the interplanar distance oscillations propagate into the structure.

B. Cleavage energies

Energies required to create pairs of complimentary $BaZrO_3$ (011) surfaces were calculated using formulas (1) and (2) and collected in Table IX. For comparison, we added values for cleavage of $BaZrO_3$ perpendicular to the [001] direction. Unit cells for slabs with the (001)-surface terminations were studied in Ref. 6. The largest cleavage energy was

TABLE VII. Mulliken charges of Ba, Zr, and O for substitution (011) terminations. I, II, III, IV, and V give the number of the layer counted from the surface. Values in parentheses show deviations from respective values in the crystal bulk. The superscript asterisk marks Ba ion in Zr site and Zr ion in Ba site. Charge deviation for this Ba calculated with respect to the bulk Zr charge.

Layer	Atomic charges (e)			Layer charge per unit cell (e)
	Zr^*/Ba	Ba^*/Zr	O	
Ba_2O-*terminated*:				
Ba_2O (I)	1.150 (−0.535)	1.040 (−0.867)*	−1.052 (0.145)	1.138 (−1.257)
O_2 (II)			−1.097 (0.100)	−2.193 (0.202)
BaZrO (III)	1.598 (−0.087)	1.850 (−0.057)	−1.210 (0.013)	2.238 (−0.157)
O_2 (IV)			−1.212 (−0.015)	−2.424 (−0.029)
BaZrO (V)	1.694 (0.009)	1.979 (0.072)	−1.190 (0.007)	2.483 (0.088)
O_2/Zr_2O-*terminated*:				
O_2 (I)			−0.973 (0.225)	−1.945 (0.450)
Zr_2O (II)	1.839 (0.154)*	2.196 (0.289)	−1.155 (0.042)	2.881 (0.486)
O_2 (III)			−1.125 (0.072)	−2.251 (0.144)
BaZrO (IV)	1. 655 (−0.030)	1. 967 (0.060)	−1.141 (0.056)	2.480 (0.085)
O_2 (V)			−1.165 (0.032)	−2.330 (0.065)

obtained for a pair of Ba_2O- and O_2/Zr_2O-terminated (011) surfaces. This is not a surprise, because the cleavage energy for this pair of surfaces includes the energy required to switch positions of Ba and Zr atoms. Obviously, it is hard to expect formation of such surfaces during cleavage. We provide this value only for comparison with the cleavage energies for creation of other pairs of surfaces. Both pairs of surfaces stabilized through removal of ions have smaller cleavage energies than the pair of BaZrO- and O_2-terminated (011) surfaces, which are created by splitting a $BaZrO_3$ crystal between two different (011) crystal planes and stabilized by strong electron redistribution. It seemed that creation of

TABLE VIII. Interplanar distances and rumpling on substitution (011) terminations. Positions of crystal planes are computed by averaging the coordinates of the corresponding atoms. The superscript asterisk marks Ba ion in Zr site and Zr ion in Ba site. The interplanar distances are given in angstroms and their variations with respect to the bulk value are provided in parentheses (in percents of interplanar distances in the bulk). Rumpling is determined as the distance between the atom and respective crystal plane.

Layer	Interplanar distances (Å)	Rumpling (Å)		
		Zr^*/Ba	Ba^*/Zr	O
Ba_2O-*terminated*:				
Ba_2O (I)		−0.43	0.65	−0.22
⇕	1.40 (−7%)			
O_2 (II)				0
⇕	1.57 (+5%)			
BaZrO (III)		0.10	−0.06	−0.04
⇕	1.51 (+1%)			
O_2 (IV)				0
⇕	1.50 (0%)			
O_2/Zr_2O-*terminated*:				
O_2 (I)				0
⇕	0.87 (−42%)			
Zr_2O (II)		0.17	−0.10	0.08
⇕	1.74 (+16%)			
O_2 (III)				0
⇕	1.19 (−21%)			
BaZrO (IV)		−0.12	−0.11	0.23
⇕	1.68 (+12%)			

TABLE IX. Calculated cleavage energies.

Created pairs of surfaces	Cleavage energy (eV/unit cell)	Cleavage energy (J/m^2)
$BaZrO(011)+O_2(011)$	6.147	3.865
$O(011)+O(011)$	3.267	2.054
$ZrO(011)+Ba(011)$	3.672	2.309
$Ba_2O+O_2/Zr_2O(011)$	9.482	5.963
$BaO(001)+ZrO_2(001)$	1.316	1.170

defects is a preferable way for stabilization of $BaZrO_3$ (011) surfaces. The lowest cleavage energy is found for the creation of a complimentary pair of O-terminated (011) surfaces. Therefore, one should expect formation of these surfaces, when a $BaZrO_3$ crystal is cleaved perpendicular to the [011] direction. However, the crystal splitting perpendicular to the [001] direction requires half the energy of the O-terminated (011) surface. Thus a more realistic expectation is that an attempt to cleave $BaZrO_3$ perpendicular to the [011] direction will lead to saw-shaped surface formation with each step oriented perpendicular to the [001] direction, or to breaking of the crystal to pieces terminated by (001) surfaces. The following evolution of these surfaces depends on possibilities of ion exchange between crystal bulk and surface, surface and environment, and mobility of atoms on the surface.

C. Stability of surfaces with different terminations

We have calculated the excess [see Eq. (8)] of oxygen and Ba atoms with respect to Zr atoms in the simulated slabs and ϕ^i values according to definition (33). The results are collected in Table X. These data determine SGFEs for all considered (011) surface terminations of a $BaZrO_3$ crystal. In addition, we provide data obtained for $BaZrO_3$ (001) surfaces. The most stable surface for any particular value of the Ba and O chemical potentials is the surface with the smallest SGFE value. The regions of stability for different surface terminations are presented on phase diagrams shown on the left side of Figs. 4(a) and 4(b). Figure 4(a) compares different terminations of BaZrO3 (011) surfaces. Figure 4(b) includes also comparison with BaO- and ZrO_2-terminated $BaZrO_3$ (001) surfaces. Boundaries between the regions of stability for different terminations are marked by dashed lines. The boundary between stability regions for surfaces with terminations $\boldsymbol{i}$ and $\boldsymbol{j}$ is determined by solution of the equation

$$\Omega^i(\Delta\mu_{\mathrm{Ba}},\Delta\mu_{\mathrm{O}}) = \Omega^j(\Delta\mu_{\mathrm{Ba}},\Delta\mu_{\mathrm{O}}). \tag{35}$$

The solutions differ from each other only by a constant on the right side of the equation for all significant cases:

$$\Delta\mu_{\mathrm{Ba}} + \Delta\mu_{\mathrm{O}} = g(i,j). \tag{36}$$

The constants $g(i,j)$ for different boundaries are assembled in Table XI. All boundaries appeared to be parallel.

Pure $BaZrO_3$ surfaces exist only when conditions (19)–(22) are satisfied. These conditions are shown in Fig. 4 by solid lines, which indicate where precipitation of Ba, Zr, and their oxides occurs. The formation energies of $BaZrO_3$ and barium and zirconium oxides, which determine positions of respective precipitation lines, are given in Table XII. These energies agree with experimental data shown in the same table reasonably well. Precipitation of zirconium metal occurs below the Zr precipitation line. Barium precipitates on the right from the Ba precipitation line. BaO crystals will grow on the right and above the BaO precipitation line, while ZrO_2 will grow below and on the left from the ZrO_2 precipitation line. The only region where a pure $BaZrO_3$ surface can be obtained is the narrow stripe between the BaO precipitation line on the right and the ZrO_2 precipitation line on the left. At the bottom of the diagram the stripe is limited by the Zr precipitation line and by a small fragment of the Ba precipitation line. Clusters of Ba, Zr, BaO, and ZrO_2 will grow for all chemical potentials outside this narrow region.

TABLE X. Excesses of O and Ba atoms in slabs with respect to Zr atoms [Eq. (8)] and free energy of formation [Eq. (33)] for various $BaZrO_3$ (011) and (001) surfaces. These data are used to draw Figs. 4–7.

Surface $\boldsymbol{i}$	$\Gamma^i_{\mathrm{Zr,O}}$	$\Gamma^i_{\mathrm{Zr,Ba}}$	ϕ^i (eV/unit cell)	ϕ^i (J/m^2)
O_2/Zr_2O-term. (011)	−2	−2	20.58	12.94
Ba_2O-term. (011)	2	2	−7.92	−4.98
BaZrO-term. (011)	−1	0	8.00	5.03
O-term. (011)	0	0	1.95	1.23
ZrO-term. (011)	−1	−1	8.76	5.51
O_2-term. (011)	1	0	2.63	1.65
BaO-term. (001)	0.5	0.5	−2.16	−1.36
ZrO_2-term. (001)	−0.5	−0.5	4.54	2.85

A bulk $BaZrO_3$ crystal will not be sustained due to spontaneous surface formation beyond the boundaries (34) where SGFE becomes equal to zero. If we restrict our consideration to only (011) surfaces, Eq. (34) must be solved for ZrO- and Ba_2O-terminated (011) surfaces, producing the range of a $BaZrO_3$ bulk crystal existence as

$$-8.76\ \mathrm{eV} < \Delta\mu_{\mathrm{Ba}} + \Delta\mu_{\mathrm{O}} < -3.96\ \mathrm{eV}. \tag{37}$$

Inclusion of (001) surfaces into consideration leads to a decrease of the upper bound, because SGFE for the BaO-terminated (001) surface intercepts zero at smaller chemical potentials. The inequality (37) then becomes

$$-8.76\ \mathrm{eV} < \Delta\mu_{\mathrm{Ba}} + \Delta\mu_{\mathrm{O}} < -4.32\ \mathrm{eV}. \tag{38}$$

Bounds (37) and (38) are plotted in Figs. 4(a) and 4(b), respectively.

At each point on the diagrams $BaZrO_3$ surfaces are in equilibrium with oxygen gas. The equilibrium is characterized by the oxygen chemical potential. Since a single value for the chemical potential can correspond to a wide spectrum of various temperatures and pressures, we draw dependencies of the oxygen chemical potentials on temperature for a number of gas pressures on the right side of Figs. 4(a) and

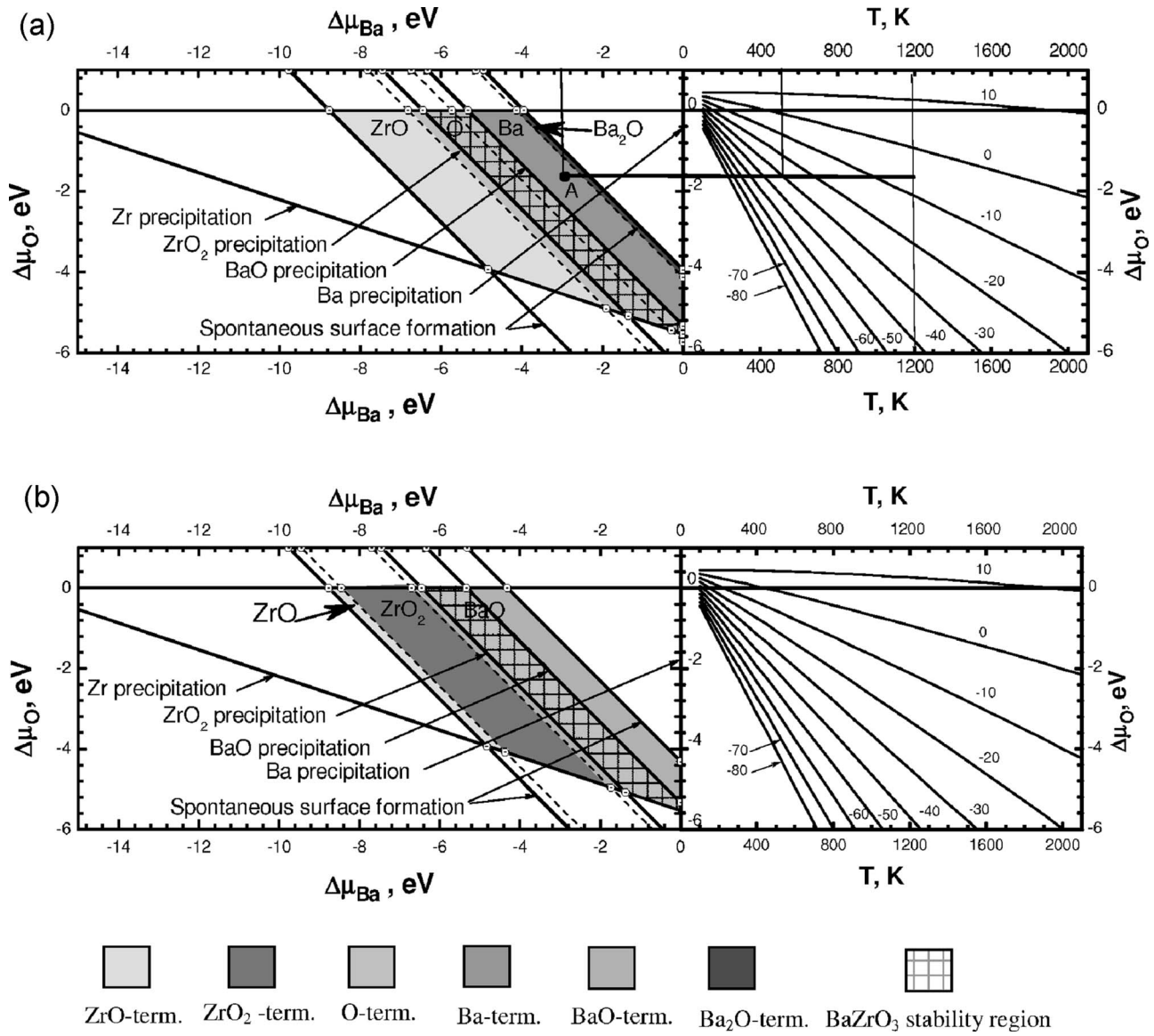

FIG. 4. Phase diagrams: The regions of stability of $BaZrO_3$ surfaces with different terminations [O_2/Zr_2O-, ZrO-, O-, Ba-, Ba_2O-terminated (011) surfaces and BaO- and ZrO_2-terminated (001) surfaces] as functions of chemical potential variations for barium (15) and oxygen (27) atoms. (a) Comparison of (011) surfaces only; (b) includes comparison of (011) and (001) surfaces. Parameters for all lines on the left side of the figures are collected in Tables X–XII and Eqs. (37) and (38). The right side of the figures contains a family of $\Delta\mu_O$ as functions of temperature at various oxygen gas pressures according to Eq. (27). The labels m on the lines represent the pressure: $p_{O_2}=10^m$ atm.

4(b). These functions were calculated from experimental data, taken from the thermodynamical tables[46] following the approach described earlier by formulas (26)–(31). The corrections (31) calculated for BaO ($\delta\mu_O^0=0.038$ eV) and for ZrO_2 ($\delta\mu_O^0=0.267$ eV) appear to be noticeably different. The variation of the correction (~0.23 eV) is very similar to the variation obtained in Ref. 27. We used an average value, $\delta\mu_O^0=0.152$ eV, to calculate the oxygen chemical potentials.

The design employed for building diagrams in Fig. 4 allows us to determine conditions for the oxygen environment, which correlate with points on the phase diagrams on the left side of the figures. For example, if we suppose the system has a temperature of 1000 K and we are interested in knowing at what pressure the oxygen gas will be in equilibrium with the surface, a vertical line is drawn at $T=1000$ K on the right side of the figures. The intercepts of the plotted functions with this line form a scale for the gas pressure. Then for any point A [Fig. 4(a)] we can determine the equilibrium gas pressure. Similarly, if the gas is under any particular pressure (for example, at 10^{-20} atm), we isolate the intercept of the horizontal line, originating from the point A with the functions for the oxygen chemical potential corresponding to that pressure. The projection of this intercept on the temperature axis provides the equilibrium temperature.

To illustrate behavior of SGFEs for different $BaZrO_3$ surfaces we have plotted Gibbs free energies for several specific conditions. In all cases, the temperature was set to 1000 K. SGFEs for the oxygen gas pressure equal to 1 atm are plot-

TABLE XI. Positions of boundaries between stability regions of surfaces with different terminations according to Eqs. (35) and (36). These data are used to draw Fig. 4.

Surface i	Surface j	$g(i,j)$
O_2/Zr_2O (011)	ZrO (011)	−11.81
ZrO (011)	O (011)	−6.81
O (011)	Ba (011)	−5.73
Ba (011)	Ba_2O (011)	−4.13
ZrO (011)	ZrO_2 (001)	−8.44
ZrO_2 (001)	BaO (001)	−6.70
BaO (001)	Ba_2O (011)	−3.84

ted in Fig. 5. Figure 6 contains SGFEs along the BaO precipitation line, and Fig. 7 shows SGEFs along the ZrO_2 precipitation line.

At smaller Ba chemical potentials (corresponding to Ba-poor conditions) the most stable surface is ZrO terminated. Under conditions with larger barium chemical potentials (that is toward the Ba-rich environment), O-, Ba-, and, finally, Ba_2O-terminated (011) surfaces become stable [Figs. 4(a) and 5]. If (001) surfaces are included in this comparison, the regions of stability will appear in the following order: ZrO-terminated (011) surfaces, followed by ZrO_2- and BaO-terminated (001) surfaces [Figs. 4(b) and 5]. The (001) surfaces are more stable than the O- and Ba-terminated (011) surfaces. Within the narrow stripe where the pure $BaZrO_3$ surface can exist, only the O- and Ba-terminated surfaces among the (011) surfaces can be stable. When the (001) surfaces are also taken into consideration, it appears that only the BaO-terminated surface is stable. This finding differs significantly from the case of $SrTiO_3$, where both SrO- and TiO_2-terminated (001) surfaces can be stable within the region of stability of a $SrTiO_3$ crystal.[27,28,36] However, the boundary between the BaO- and ZrO_2-terminated (001) surfaces lies very close to the ZrO_2 precipitation line outside the region of the $BaZrO_3$ stability. This location of the boundary means that ZrO_2 grows on the $BaZrO_3$ surface as small crystals, but not in layer-by-layer fashion, because the precipitation of ZrO_2 as small crystals leads to smaller Gibbs free energy. There is a chance that more precise computations will put this boundary inside the region of $BaZrO_3$ stability. The SGFE for the O_2/Zr_2O-terminated surface becomes the

TABLE XII. Formation energies for oxides and $BaZrO_3$ calculated according to Eqs. (18), (23), and (24). These data are used to draw Figs. 4–7.

Crystal	Calculated formation energy Δg_f (eV)	Experimental Gibbs energy of formation ΔG^0_f (eV)
BaO	−5.33	−5.39,[a] −5.44[b]
ZrO_2	−10.16	−10.81,[a] −10.78[b]
$BaZrO_3$	−16.62	−17.56[b]

[a]Reference 50.
[b]Reference 51.

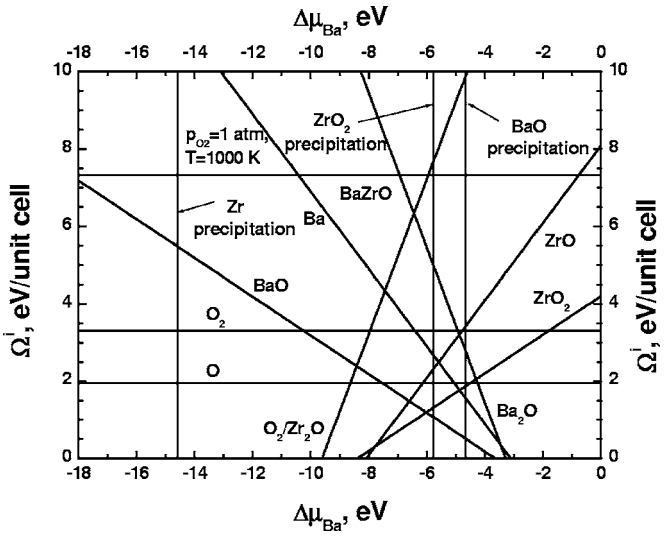

FIG. 5. Surface Gibbs free energies as a function of $\Delta\mu_{Ba}$ at $T=1000$ K and $p_{O_2}=1$ atm.

smallest beyond the region where the bulk of $BaZrO_3$ can exist, and therefore, this surface never occurs.

The Gibbs free energies for all studied surfaces, except for the O_2- and BaZrO-terminated (011) surfaces, have a constant value along the BaO and ZrO_2 precipitation lines (Figs. 6 and 7). The Gibbs free energy for the BaO-terminated (001) surface has the lowest value at both precipitation lines within the region of the $BaZrO_3$ stability. The

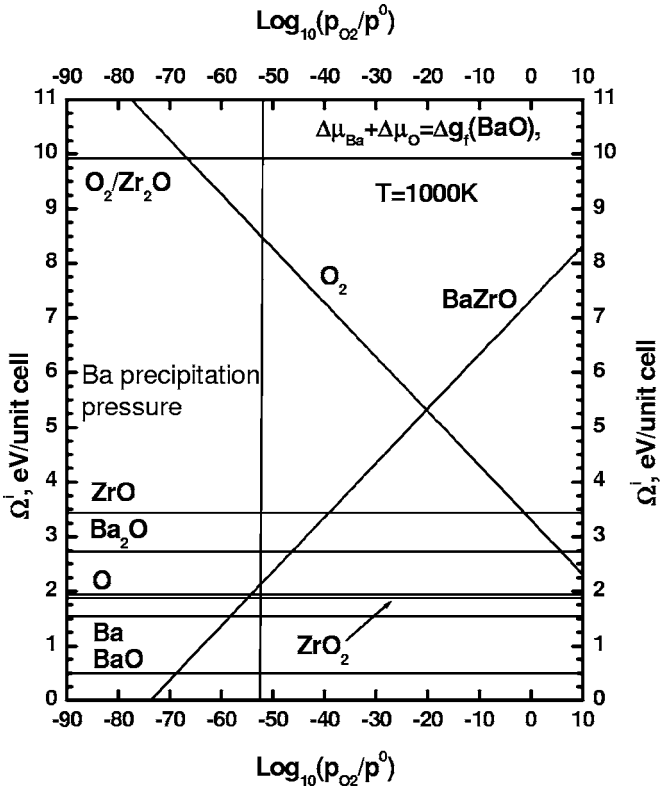

FIG. 6. Surface Gibbs free energies as a function of $\log_{10}(p_{O_2}/p^0)$ at $T=1000$ K and $\Delta\mu_{Ba}+\Delta\mu_O=\Delta g_f(BaO)$ (along BaO precipitation line).

Gibbs free energies for the O_2- and BaZrO-terminated (011) surfaces become the lowest far beyond the boundaries of the $BaZrO_3$ stability region.

IV. CONCLUSION

We used DFT calculations and thermodynamical methods to analyze possible structures of $BaZrO_3$ (011) surfaces. The new substitution type of possible surface terminations has been introduced. These terminations are formed by replacement of one type of cations with another. The exchange of ions provides a charge compensation to make the surfaces stable and prevent formation of spurious electric fields. In addition, we also included results from our previous study of (001) $BaZrO_3$ surfaces into the present analysis.

It seems that an attempt to cleave a $BaZrO_3$ crystal perpendicular to the [011] direction will lead to destruction of the crystal or formation of saw-shaped surfaces terminated with (001) surfaces. This behavior would be favored because the cleavage energy for creation of a pair of the $BaZrO_3$ (001) surfaces is much smaller than the cleavage energy for creation of any pair of (011) surfaces. If (001) surfaces are excluded from the consideration, then we would come to the conclusion that two O-terminated (011) surfaces would be created during the cleavage.

Comparison of surface Gibbs free energies for different surface terminations showed that among the potential (011) surfaces, only O- and Ba-terminated surfaces can be stable within the range of stability of a $BaZrO_3$ crystal. If the comparison includes (001) surfaces, the BaO-terminated (001) surface becomes the only stable surface termination under the conditions where bulk $BaZrO_3$ crystal is also sustainable. This finding strongly contrasts with all previous results for $SrTiO_3$ surfaces, where both (001) surface terminations (SrO and TiO_2) are possible under conditions where the bulk $SrTiO_3$ is also stable. An additional conclusion made from the present simulation is that under BaO-poor conditions (which are the same as ZrO_2-rich conditions) ZrO_2 grows as small crystals but not as layers.

Our analysis has been made for the condition of thermodynamical equilibrium and assumption that all atoms are capable of diffusion, so that the thermodynamical equilibrium can be reached. If this condition is not fulfilled, then different surfaces can also be produced on the basis, for example, that some (011) surfaces can become accessible due to kinetic reasons.

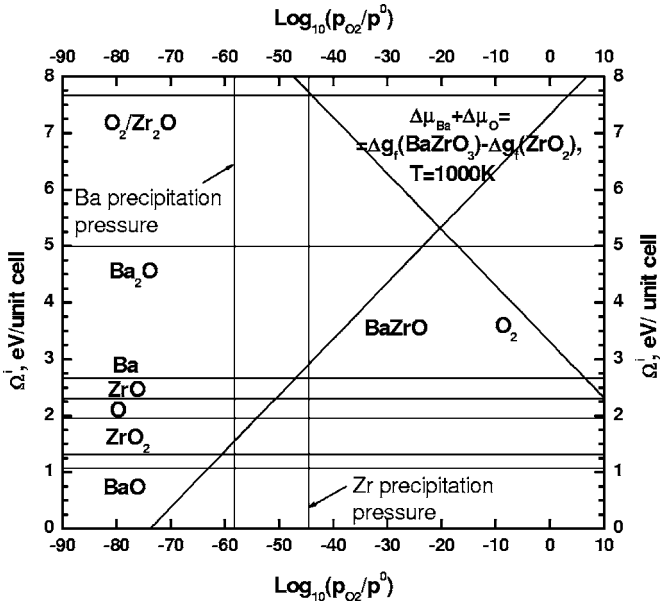

FIG. 7. Surface Gibbs free energies as a function of $\log_{10}(p_{O_2}/p^0)$ at $T=1000$ K and $\Delta\mu_{Ba}+\Delta\mu_O=\Delta g_f(BaZrO_3)-\Delta g_f(ZrO_2)$ (along ZrO_2 precipitation line).

Finally, our simulations provide ground for further theoretical studies of $BaZrO_3$ surfaces, such as studies of (111) surfaces and possible surface reconstructions, and chemical processes on $BaZrO_3$ surfaces. We hope our investigation will stimulate experimental studies of $BaZrO_3$ surfaces.

ACKNOWLEDGMENTS

This work was partly supported by the US Department of Energy under Grant No. DE-FC26-02NT41631. We thank E. A. Kotomin and S. Piskunov for fruitful discussions.

*Email address: heifets@wag.caltech.edu
†Email address: merinov@wag.caltech.edu

[1] S. M. Haile, G. Staneff, and K. H. Ryu, J. Mater. Sci. **36**, 1149 (2001).
[2] A. Erb, E. Walker, J. Y. Genoud, and R. Flukiger, Physica C **282**, 459 (1997).
[3] Y. X. Wang, M. Arai, and T. Sasaki, Appl. Phys. Lett. **88**, 091909 (2006).
[4] J. P. Desclaux, Comput. Phys. Commun. **9**, 31 (1975).
[5] J. P. Perdew, K. Burke, and M. Ernzerhof, Phys. Rev. Lett. **77**, 3865 (1996).
[6] J. Ho, E. Heifets, and B. Merinov, Surf. Sci. **601**, 490 (2007).
[7] N. Bickel, G. Schmidt, K. Heinz, and K. Müller, Phys. Rev. Lett. **62**, 2009 (1989).
[8] T. Hikita, T. Hanada, M. Kudo, and M. Kawai, Surf. Sci. **287/288**, 377 (1993).
[9] M. Kudo, T. Hikita, T. Hanada, R. Sekine, and M. Kawai, Surf. Interface Anal. **22**, 412 (1994).
[10] Y. Kido, T. Nashimura, Y. Hoshido, and H. Mamba, Nucl. Instrum. Methods Phys. Res. B **161**, 371 (2000).
[11] W. C. Mackrodt, Phys. Chem. Miner. **15**, 228 (1988).
[12] J. Prade, U. Schroder, W. Kress, F. W. de-Wette, and A. D. Kulkarni, J. Phys.: Condens. Matter **5**, 1 (1993).
[13] E. Heifets, S. Dorfman, D. Fuks, E. Kotomin, and A. Gordon, Surf. Rev. Lett. **5**, 341 (1998).
[14] E. Heifets, S. Dorfman, D. Fuks, and E. Kotomin, Thin Solid Films **296**, 76 (1997).
[15] E. Heifets, S. Dorfman, D. Fuks, E. Kotomin, and A. Gordon, J.

Phys.: Condens. Matter **10**, L347 (1998).
[16] E. Heifets, E. A. Kotomin, and J. Maier, Surf. Sci. **462**, 19 (2000).
[17] J. Padilla and D. Vanderbilt, Surf. Sci. **418**, 64 (1998).
[18] J. Padilla and D. Vanderbilt, Phys. Rev. B **56**, 1625 (1997).
[19] B. Meyer, J. Padilla, and D. Vanderbilt, Faraday Discuss. **114**, 395 (1999).
[20] F. Cora, and C. R. A. Catlow, Faraday Discuss. **114**, 421 (1999).
[21] R. E. Cohen, Ferroelectrics **194**, 323 (1997).
[22] L. Fu, E. Yaschenko, L. Resca, and R. Resta, Phys. Rev. B **60**, 2697 (1999).
[23] C. Cheng, K. Kunc, and M. H. Lee, Phys. Rev. B **62**, 10409 (2000).
[24] E. Heifets, R. I. Eglitis, E. A. Kotomin, J. Maier, and G. Borstel, Phys. Rev. B **64**, 235417 (2001).
[25] E. A. Kotomin, R. I. Eglitis, J. Maier, and E. Heifets, Thin Solid Films **400**, 76 (2001).
[26] S. Piskunov, E. A. Kotomin, E. Heifets, J. Maier, R. I. Eglitis, and G. Borstel, Surf. Sci. **575**, 75 (2005).
[27] K. Johnston, M. R. Castell, A. T. Paxton, and M. W. Finnis, Phys. Rev. B **70**, 085415 (2004).
[28] C. Noguera, J. Phys.: Condens. Matter **12**, R367 (2000).
[29] H. Bando, Y. Ochiai, Y. Aiura, Y. Haruyama, T. Yasue, and Y. Nishihara, J. Vac. Sci. Technol. A **19**, 1938 (2001).
[30] J. Brunen and J. Zegenhagen, Surf. Sci. **389**, 349 (1997).
[31] K. Szot and W. Speier, Phys. Rev. B **60**, 5909 (1999).
[32] A. Pojani, F. Finocchi, and C. Noguerra, Surf. Sci. **442**, 179 (1999).
[33] A. Stashans and S. Serrano, Surf. Sci. **497**, 285 (2002).
[34] E. Heifets, E. A. Kotomin, and J. Maier, Surf. Sci. **462**, 19 (2000).
[35] F. Bottin, F. Finocchi, and C. Noguera, Phys. Rev. B **68**, 035418 (2003).
[36] E. Heifets, W. A. Goddard III, E. A. Kotomin, R. I. Eglitis, and G. Borstel, Phys. Rev. B **69**, 035408 (2004).
[37] K. Reuter and M. Scheffler, Appl. Phys. A: Mater. Sci. Process. **78**, 793 (2004).
[38] K. Reuter and M. Scheffler, Phys. Rev. B **65**, 035406 (2001).
[39] X. G. Wang, A. Chaka, and M. Scheffler, Phys. Rev. Lett. **84**, 3650 (2000).
[40] X. G. Wang, W. Weiss, S. K. Shaikhutdinov, M. Ritter, M. Petersen, F. Wagner, R. Schlögl, and M. Scheffler, Phys. Rev. Lett. **81**, 1038 (1998).
[41] http://www.cs.sandia.gov/~paschul/Quest/SeqQ_Home.html.
[42] The files with basis sets and pseudopotentials in the format suitable for SeqQuest code (Ref. 41) are available on request. Oxygen pseudopotential and basis set (unpublished) were developed by P. Schultz at Sandia Laboratory (see web site in Ref. 41). The pseudopotentials and basis sets for Ba and Zr (unpublished) were developed by M. Uludogan and H.-J. Lee, respectively, in Materials Simulation Center at California Institute of Technology.
[43] N. Troullier and J. L. Martins, Phys. Rev. B **43**, 8861 (1991).
[44] D. R. Hamann, Phys. Rev. B **40**, 2980 (1989).
[45] S. G. Louie, S. Froyen, and M. L. Cohen, Phys. Rev. B **26**, 1738 (1982).
[46] *NIST Chemistry WebBook, NIST Standard Reference Database No. 69*, edited by P. J. Linstrom and W. G. Mallard (National Institute of Standards and Technology, Gaithersburg, MD, 2003), http://webbook.nist.gov/chemistry/.
[47] H. D. Megaw, Z. Phys. Chem. Abt. B **28**, 65 (1935).
[48] O. I. Prokopalo, I. P. Raevskii, M. A. Malitskaya, Yu. M. Popov, A. A. Bokov, and V. G. Smotrakov, Ferroelectrics **45**, 89 (1975).
[49] J. Robertson, J. Vac. Sci. Technol. B **18**, 1785 (2000).
[50] *CRC Handbook of Chemistry and Physics*, 81th ed. (CRC Press, Boca Raton, FL, 2000).
[51] I. Barin, *Thermochemical Data of Pure Compounds*, 3rd ed. (VCH Verl. Ges., Weinheim, 1995).